



Article

# Antibacterial Functionalization of PVD Coatings on Ceramics

Javier Osés <sup>1,2,\*</sup>, Gonzalo García Fuentes <sup>1,2</sup>, José Fernández Palacio <sup>1</sup>, Joseba Esparza <sup>1</sup>, José Antonio García <sup>2</sup>  and Rafael Rodríguez <sup>2,3</sup> 

<sup>1</sup> Centro de Ingeniería Avanzada de Superficies, Asociación de la Industria Navarra, Carretera de Pamplona 1, 31191 Cordovilla, Spain; gffuentes@ain.es (G.G.F.); jfpalacio@ain.es (J.F.P.); jegorraiz@ain.es (J.E.)

<sup>2</sup> Departamento de Ingeniería, Universidad Pública de Navarra—UPNA, Campus Arrosadía s/n, 31006 Pamplona, Spain; joseantonio.garcia@unavarra.es (J.A.G.); rafael.rodriguez@unavarra.es (R.R.)

<sup>3</sup> INAMAT Institute for Advanced Materials, Universidad Pública de Navarra—UPNA, Campus Arrosadía s/n, 31006 Pamplona, Spain

\* Correspondence: joses@ain.es; Tel.: +34-948-421-101

Received: 31 March 2018; Accepted: 17 May 2018; Published: 22 May 2018



**Abstract:** The application of surface treatments that incorporate silver or copper as antibacterial elements has become a common practice for a wide variety of medical devices and materials because of their effective activity against nosocomial infections. Ceramic tiles are choice materials for cladding the floors and walls of operation rooms and other hospital spaces. This study is focused on the deposition of biocide physical vapor deposition (PVD) coatings on glazed ceramic tiles. The objective was to provide antibacterial activity to the surfaces without worsening their mechanical properties. Silver and copper-doped chromium nitride (CrN) and titanium nitride (TiN) coatings were deposited on samples of tiles. A complete characterization was carried out in order to determine the composition and structure of the coatings, as well as their topographical and mechanical properties. The distribution of Ag and Cu within the coating was analyzed using glow discharge optical emission spectrometry (GD-OES) and field emission scanning electron microscope (FE-SEM). Roughness, microhardness, and scratch resistance were measured for all of the combinations of coatings and dopants, as well as their wettability. Finally, tests of antibacterial efficacy against *Staphylococcus aureus* and *Escherichia coli* were carried out, showing that all of the doped coatings had pronounced biocide activity.

**Keywords:** silver; copper; TiN; CrN; ceramic tiles

## 1. Introduction

A growing body of scientific evidence has demonstrated the key role that environmental surfaces play in the transmission of nosocomial infections. A broad spectrum of pathogens can persist in the environment for hours to days, contaminating surfaces and equipment in hospital rooms and eventually colonizing the hands of health care personnel [1–3].

Biocide and self-disinfecting surfaces have received a major attention in the recent years, and are considered the most effective solution to the problem [4,5]. Surface treatments and coatings provide a wide range of strategies that have to be tailored to the characteristics of each substrate and environment.

The biocide activity of some heavy metals, particularly silver [6] and copper [7], has been extensively used in many situations, even before the clinical introduction of antibiotics in the 1940s. Coatings that incorporate these elements as metallic ions, compounds, or nanoparticles can eventually be used as antibacterial protective layers [8,9].

Ceramic tiles are choice materials for cladding the floors and walls of operation rooms and other hospital spaces. A biocide coating that is deposited on top of the glazed surface should also share the high mechanical properties of the ceramic substrate. Physical vapor deposition (PVD) coatings meet these requirements. Moreover, the interest in new decorative finishings in the ceramic industry has already consolidated the massive use of PVD technologies to provide metallic appearance to a great variety of tiles [10]. Well-adhered hard coatings can be easily deposited at an affordable cost. We just need to dope them with biocide elements to obtain the required combination of mechanical properties and antibacterial functionality.

Some previous works have presented doping technologies such as ion implantation that allow achieving the desired combination of properties [11,12], although the need of a cost-effective solution suggests that it would be better to combine the deposition and the doping of the coating in one process. The co-evaporation of silver or copper during the last step of the deposition process of PVD hard coatings could provide antibacterial capacity. The PVD ceramic coating is not able to dissolve a high amount of metal, so the produced structure is a composite ceramic-metal. The metal segregates in the grain boundary, and also appears as microdroplets in the coating [13,14].

For that reason, the induced changes in the mechanical properties of the whole layer should be controlled in order to prevent the worsening of their tribo-mechanical performance. Some previous papers already have shown that the addition of these soft and ductile metals can reduce the friction coefficient [15,16], although each particular property has to be checked for the coatings deposited on different substrates.

It also must be taken into account that bacteria also colonize the mortar that is used to fix the ceramic tiles; thus, these treatments have to be combined with the use of antibacterial mortars in order to ensure the sterile environment. Some additives based on the use of silver can be added to conventional mortars with the aim of obtaining the antibacterial effect [17,18].

This paper presents a systematic study of the mechanical and antibacterial properties of the combinations of two hard coatings—chromium nitride (CrN) and titanium nitride (TiN)—with two biocide metals (Ag and Cu) co-deposited during a single process on standard glazed ceramic tiles.

## 2. Materials and Methods

### 2.1. Materials

Common white glazed ceramic tiles were prepared as substrate for the coating process. Tiles of  $10 \times 10 \text{ cm}^2$  in area and 0.5 cm in thickness were cut to obtain  $5 \times 5 \text{ cm}^2$  samples. This size was suitable for the coating and the characterization process.

Pristine samples, without further treatment, were tested and used as reference for the rest of PVD-treated samples. This data will be compared with the data obtained in the characterization of the different PVD coatings.

For glow discharge optical emission spectrometry (GD-OES) tests, electrically conductive substrates were needed. In these cases, F521 steel round samples that were 3 cm in diameter and 0.5 cm in thickness were used. These samples were mirror polished up to a surface roughness average ( $R_a$ ) of about 10 nm, using grinding papers of silicon carbide and cloths with diamond suspension.

### 2.2. Deposition Process

The samples were cleaned using n-propanol and dried in an oven at 80 °C for 6 h. This process was repeated three times in order to eliminate all of the possible contamination on the surface. The metallic samples were cleaned with n-propanol in an ultrasonic bath, and then dried in an oven at 80 °C for 6 h.

After the cleaning process, three groups of 15 ceramic samples and one metallic sample were introduced in the PVD chamber for the CrN-based coatings, and identical batches were used for the TiN-based coatings.

METAPLAS IONON MZR 323 PVD equipment (Metaplas Ionon GmbH, Gladbach, Germany) was used to deposit the coatings. The chamber size of this equipment is 400 mm  $\varnothing$   $\times$  500 mm, has six evaporators, and all of the parameters and gas intakes are controlled by METAPLAS software.

Cathodic arc was used to evaporate the metals (Cr, Ti/Ag, Cu) in the PVD chamber. CrN and TiN were formed introducing a nitrogen flow in the chamber during the evaporation of the metals. To obtain the different coatings, the metallic cathodes (five of chromium/titanium and one of silver/copper) were changed for each of the six deposition processes, using the same deposition parameters. The CrN-based coatings were: CrN, CrN+Ag, and CrN+Cu. The same scheme was repeated for the TiN-based coatings, by employing Ti cathodes instead of the Cr that was used in the previous series. The obtained coatings were labeled as TiN, TiN+Ag, and TiN+Cu. A batch of 15 ceramic samples and one metallic sample was coated on each process.

The deposition process steps were:

- Vacuum  $1 \times 10^{-5}$  mbar.
- Heating up to 400–450 °C.
- Argon etching for 30 min.
- Deposition of a thin chromium (titanium) interfacial layer. During this step, a current of 60 A was applied on the five chromium (titanium) cathodes without the addition of nitrogen into the chamber.
- Deposition of CrN (TiN) layer. The same current was applied on the chromium (titanium) cathodes while a nitrogen flow of 500 sccm.
- Deposition of doped CrN (TiN) + biocide metal (Ag/Cu) layer. In this phase, the evaporation happened in the six metallic cathodes.

A schematic cross-section of the PVD coatings on the ceramic tiles is shown in Figure 1.

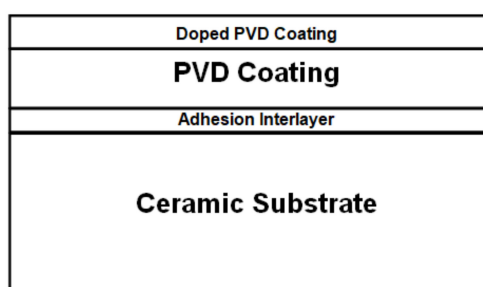


**Figure 1.** Cross-section of the deposited coatings on the ceramic tiles.

### 2.3. Chemical Characterization and Microscopy

After the deposition process, the coatings were analyzed by glow discharge optical emission spectrometry (GD-OES), using a JOBIN YVON 10000RF GD-OES equipment (HORIBA Instruments Incorporated, Irvine, CA, USA). The metallic samples were used in these tests due to their conductive nature. The conductivity of the metal allows quantifying the thickness and weight percentage of the chemical elements. Thus, the chemical composition profiles of the coatings were obtained.

The surface morphology and the distribution of the antibacterial elements were analyzed using a HITACHI S4800 field emission scanning electron microscope (FE-SEM, Hitachi High-Technologies Corporation, Tokyo, Japan). Using electron dispersive X-ray analysis (EDX) microprobe and backscattered electrons images, the distribution of the different elements was determined.

### 2.4. Thickness and Topography

The thickness of the coatings was obtained using CSM Calotest equipment (CSM Instruments, Needham, MA, USA). Tests were performed on ceramic samples using a 30-mm  $\varnothing$  stainless steel ball and CSM Superfine Diamond Water Suspension as the abrasive media.

The roughness was analyzed using a WYCO RST-500 interferometric profilometer (Veeco Corporate, Plainview, NY, USA). Measurements were carried out using the vertical scanning interferometry mode (VSI). Vertical resolution using this mode is 3 nm. Three-dimensional (3D) images of the surfaces were obtained, and the changes on  $R_a$  (surface roughness average),  $R_q$  (root mean square roughness), and  $R_t$  (maximum roughness depth) were studied.

### 2.5. Mechanical Characterization

The hardness of the coating and the hardness profiles were obtained with a FISCHERSCOPE<sup>®</sup> H100VP-XY PROG microdurometer (Helmut-Fischer GmbH, Sindelfingen, Germany) fitted with a diamond Vickers microindenter (Buehler, Lake Bluff, IL, USA). Hardness profiles were obtained measuring the surface hardness, applying 100 mN of maximum load in 100 steps in the load cycle, and 20 steps in the unload cycle. Since the depth of indentation was in excess of 1/10 of the coating thickness, the substrate could influence the measured hardness [19,20]. However, this was not the case, because the equipment employed in this study used the Doerner–Nix method [21–23], which calculates hardness from data along the loading curve, allowing the depth dependence of the hardness to be obtained from one indentation during the displacement of the indenter from 0  $\mu\text{m}$  to 0.8  $\mu\text{m}$ . At least 20 indentations were made on each sample, and the mean hardness value was calculated.

The adhesion between the coating and the substrate was measured using a CSM REVETEST Scratch Tester (CSM Instruments, Needham, MA, USA) fitted with a Rockwell indenter (diamond cone) (CSM Instruments). Using a load rate of 100 N/min and a scratching velocity of 10 mm/min, three tracks were produced on each analyzed sample. During the optical analysis of the scratches, three different critical loads (LC) are registered. The first critical load (LC1) is established when the first cohesive failure is detected. The second (LC2) is established when the first adhesive failure is detected, and finally the third critical load (LC3) is taken when total delamination of the coating is produced or a critical defect in the substrate is observed. The maximal load, in all cases was 80 N, and the length of the scratch track was 8 mm.

### 2.6. Wettability (Contact Angle)

The wettability of the samples was studied using a KRÜSS DSA 16 EasyDrop equipment (Krüss GmbH, Hamburg, Germany). An average value of the contact angle between the sample surfaces and at least five deionized water drops was measured using the sessile drop method. The static contact angle (sessile drop) was obtained using the Tangent Method 1 algorithm with an accuracy of  $\pm 0.1^\circ$ .

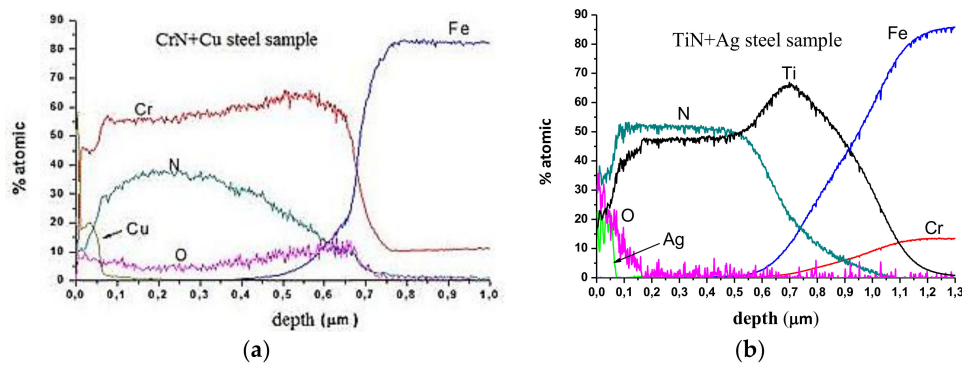
### 2.7. Antibacterial Efficacy

The antibacterial efficacy of the deposited coatings was determined following the JIS Z 2801:2010 standard [24]. The tested bacteria were *E. coli* (Gram negative) and *S. aureus* (Gram positive). The number of bacteria colonies in the TiN (reference) and the metal-doped TiN samples was compared after 24 h in a controlled media. The standard uses a factor called R that compares, in logarithmic scale, the number of colonies grown in the reference and the antibacterial surface. Coatings that presented bacteria mortality higher than 99% ( $R > 2$ ) were considered valid.

## 3. Results and Discussion

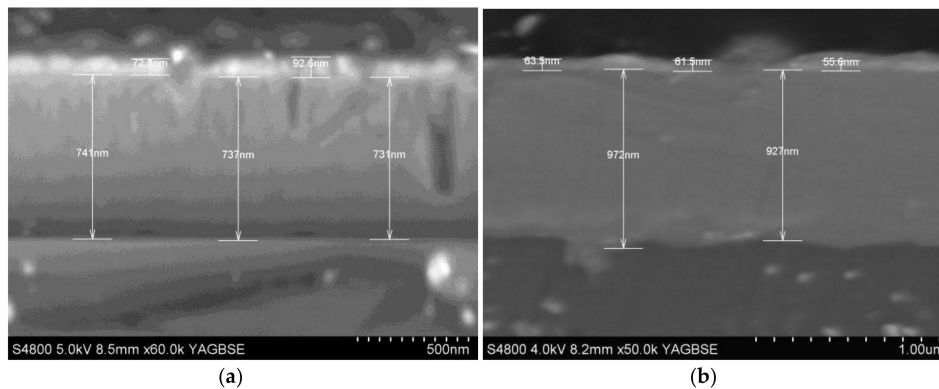
### 3.1. Chemical Characterization and Microscopy

Figure 2 shows the GD-OES profiles of the CrN+Cu and the TiN+Ag coatings. It can be observed that the deposited PVD coatings have an approximately thickness of 0.7  $\mu\text{m}$ , while the doped part of the coating has less than 100 nm, and the copper and silver content is about 20%. The other coatings (CrN+Ag and TiN+Cu) present a similar doped layer composition due to the parameters used during the deposition process, which were the same in all of the cases. TiN coatings are thicker (0.9  $\mu\text{m}$ ) due to the higher evaporation rate of the Ti with respect to the Cr.



**Figure 2.** Glow discharge optical emission spectrometry (GD-OES) composition profile of (a) chromium nitride (CrN)-Cu; (b) titanium nitride (TiN)-Ag.

A cross-section analysis that was carried out with backscattered electron images (BSE) and EDX confirmed the results obtained by GD-OES, showing the different parts of the deposited layers and the thickness of each phase (Figure 3).



**Figure 3.** Cross-section SEM image: (a) CrN+Ag; (b) TiN+Ag. The doped layer in the top of the coatings is brighter due to the silver content.

Field emission-scanning electron microscope (FE-SEM) analysis showed a heterogeneous distribution of the doping metal over all the surface of the treated surfaces.

The size of the metallic particles varied between tens of nanometer for the smallest ones to almost 10 μm for the biggest silver microdroplets. We ascribed the large size of these microdroplets to the low melting point of the antibacterial metals. Electron dispersive X-ray analysis (EDX) and backscattered electron images (BSE) confirm the composition of these particles (Figures 4–6).

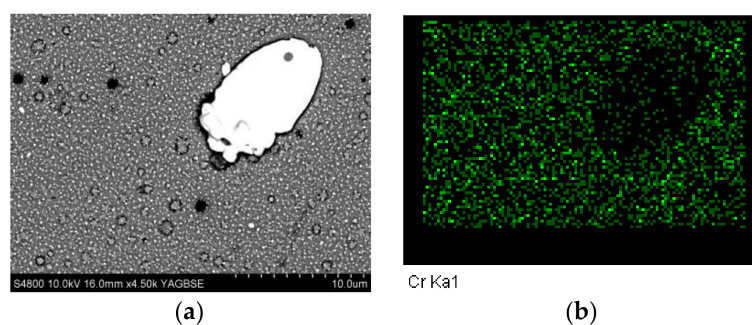


**Figure 4.** Cont.



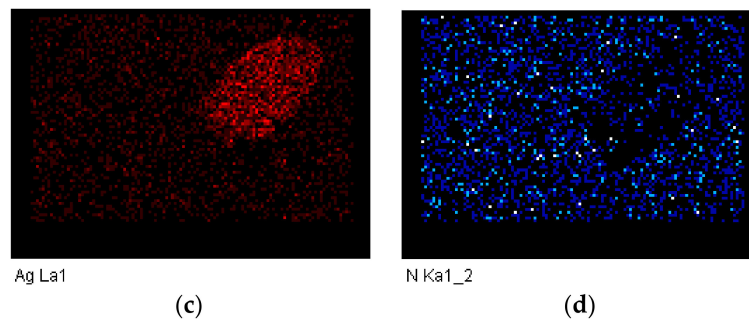


**Figure 4.** Electron dispersive X-ray (EDX) analysis of the surface of the CrN+Ag coating showing a silver microdroplet: (a) Backscattered electron images (BSE) image; (b) Chromium; (c) Silver; (d) Nitrogen.

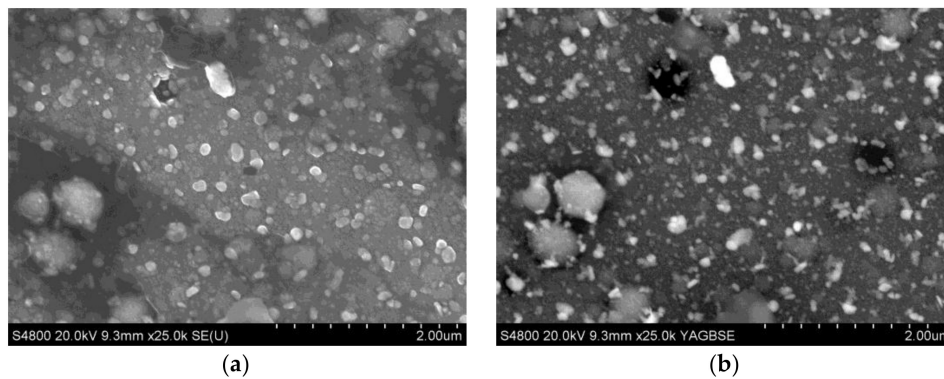


**Figure 5.** SEM images of the CrN+Ag surface: (a) Secondary electrons; (b) Backscattered electrons. The bright phase in the BSE image corresponds to silver.

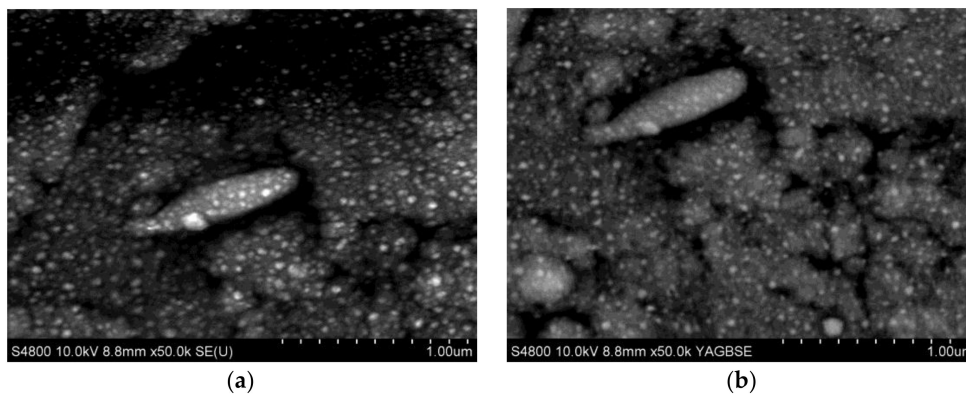


**Figure 6.** SEM images of the CrN+Cu surface: (a) Secondary electrons; (b) Backscattered electrons. The bright phase in the BSE image corresponds to copper.

### 3.2. Thickness and Topographical Characterization

After the GD-OES and FE-SEM results, the mechanical characterization of the coatings was performed. Firstly, Calotest tests were carried out to determine the thickness of the coating. All of the measured thicknesses were between 0.6–0.8  $\mu\text{m}$  (see Table 1). The small differences observed are owing to the position of the sample in the chamber during the deposition process.

Together with the thickness measurements, the roughness of the different samples was analyzed and compared. The finishing of the samples was found to be the same for all of the treatments; all of the surfaces presented a flat and metallic bright appearance.

A slight increment in the roughness of the treated samples with respect to the untreated ones was observed. However, in all of the cases, the surface has a mirror appearance. We have observed a relationship between the roughness of the sample and the melting point of the antibacterial metal. The lower the melting point of the evaporated metal, the bigger the measured roughness. For the CrN-based coatings, the smallest values correspond to the non-treated substrates and the CrN samples. The CrN+Cu samples presented slightly higher values than the previous ones, and the CrN+Ag values presented the highest roughness of all of the analyzed samples. A similar pattern is found in the case of the TiN-based coatings, although the increase in roughness due to the soft metal doping is less relevant. In both families of coatings, the co-evaporation of silver produces higher increases of the  $R_t$ , due to the size of the microdroplets (see Table 1). These roughness values are important in the wettability of the coatings, which will be discussed later.

**Table 1.** Calotest and profilometry results for CrN and TiN-based coatings.

Sample	Calotest		Profilometry	
	Thickness ( $\mu\text{m}$ )	$R_a$ (nm)	$R_q$ (nm)	$R_t$ ( $\mu\text{m}$ )
Untreated sample	–	$54 \pm 6$	$70 \pm 6$	$1.3 \pm 0.12$
CrN	$0.68 \pm 0.01$	$44 \pm 9$	$56 \pm 12$	$1.47 \pm 0.5$
CrN+Ag	$0.65 \pm 0.02$	$75 \pm 29$	$100 \pm 29$	$3.55 \pm 0.76$
CrN+Cu	$0.58 \pm 0.02$	$51 \pm 11$	$67 \pm 12$	$1.98 \pm 0.44$
TiN	$0.77 \pm 0.01$	$46 \pm 8$	$58 \pm 14$	$1.43 \pm 0.5$
TiN+Ag	$0.76 \pm 0.02$	$59 \pm 12$	$89 \pm 11$	$3.99 \pm 0.83$
TiN+Cu	$0.76 \pm 0.02$	$45 \pm 7$	$69 \pm 5$	$3.11 \pm 0.85$

The color of the treated samples is not affected significantly by the antibacterial metal. CrN samples, with and without doping, present the typical grey metallic appearance. However, the doped TiN samples present a slight change with respect to the conventional golden color, presenting a matte golden tone, due to the presence of metallic droplets in the surface.

### 3.3. Mechanical Properties

As expected, hardness tests showed an increment in the hardness of the coated samples with respect to the uncoated ceramic sample. The reason for this is that CrN and TiN are, in general, harder than common ceramic glaze (see Table 2). Figure 7 shows the hardness profiles that were obtained in the different samples studied in this paper. Due to the non-conductive nature of the ceramic substrates, direct current (DC) biasing the samples is useless, since the substrate surface will not follow the applied bias voltage, which affects the growth of the coatings, leading to hardness values that are much lower than the reference values obtained on metallic substrates (18 GPa for CrN and 24 GPa for TiN) [25]. In addition, the measured hardness of the coatings decreased rapidly with the depth of indentation, being significantly affected by the relative softness of the substrate. Meanwhile, the measured hardness of pristine slightly increased with the depth of indentation, which is due to the compression.

Concerning the effect of the Ag and Cu doping of the coatings, there is not any sensible change in the microhardness of TiN samples (see Table 2 and Figure 7). However, in the case of the CrN-based coatings, the hardness of the samples doped with silver showed, on average, higher values along all the profile, while the samples doped with copper remained below the non-doped profile. The difference in their thicknesses would explain the difference in the shapes of their curves.

Scratch tests were firstly carried out on uncoated samples with the purpose of estimating the maximum applied load that could be applied to the tiles before breaking the glaze. It was found that this maximum load was around 75N (Figure 8a). When scratch tests were performed on PVD-coated samples, the very first cohesive and adhesive defects were detected well before the limit load of 75 N. Nevertheless, for the CrN-based coatings, the adhesion was good enough to resist the scratch test until

the glaze fracture without peeling off or chipping off of the coating (Figure 8b). On the other hand, the TiN-based coatings gave lower values for all three critical loads. In particular, the TiN+Ag coating provided the lowest values for the LC2 and LC3 (see Table 2 and Figure 8c). Since the difference between the TiN and TiN+Ag samples was located on the upper part (first 100 nm), where the addition of metal changes the properties of the coating, the difference in adhesion is attributed to the problems during the cleaning process of the ceramic samples, affecting the adhesion forces between the substrate and the PVD coating due to the presence contamination in the interfacial region.

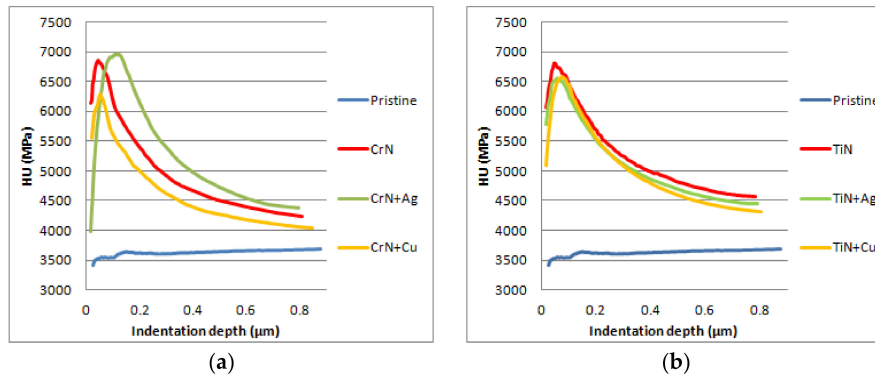


Figure 7. Hardness profiles of the coatings: (a) CrN-based coatings and (b) TiN-based coatings.

Table 2. Microhardness, scratch test, and wettability results for CrN and TiN-based coatings.

Sample	Microhardness		Scratch Test			Wettability
	UH (N/mm <sup>2</sup> )	LC1 (N)	LC2 (N)	LC3 (N)	Contact Angle (°)	
Untreated sample	3688 ± 26	15 ± 2	41 ± 1	71 ± 2	48.3 ± 1.7	
CrN	6856 ± 576	6 ± 1	25 ± 1	72 ± 2	90.7 ± 3.2	
CrN+Ag	6968 ± 442	11 ± 1	27 ± 2	70 ± 2	107.4 ± 0.7	
CrN+Cu	6278 ± 478	6 ± 1	40 ± 3	72 ± 2	115.6 ± 1.2	
TiN	6711 ± 385	6 ± 1	22 ± 2	42 ± 3	74.5 ± 2.4	
TiN+Ag	6559 ± 337	5 ± 1	12 ± 1	20 ± 3	91.3 ± 0.9	
TiN+Cu	6586 ± 333	6 ± 1	24 ± 4	44 ± 3	117.8 ± 0.4	

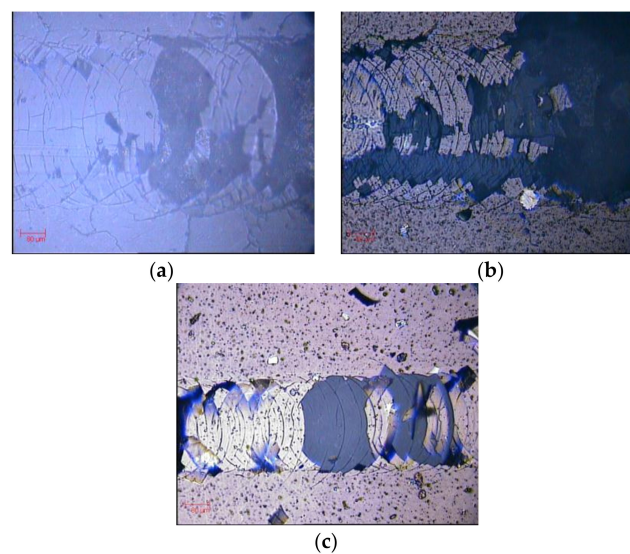


Figure 8. Scratch tests images: (a) pristine sample; (b) CrN+Ag; (c) TiN+Ag. (Scale bar in each image indicates 80 μm).



During the first part of the tests, while the indenter affected the first nanometers of the coating, no differences were detected between the doped and non-doped samples. The doped part of the layers was chemically bonded with the bulk layer, so no delaminations between sublayers were observed.

### 3.4. Wettability

Table 2 and Figure 9 resume the results of the contact angle measurements. Both PVD coatings had a higher contact angle than the uncoated ceramic, due to their lower surface energy. The measured angle increased from  $48^\circ$  for the uncoated samples to  $90^\circ$  in the case of the CrN, and to  $75^\circ$  in the case of the TiN, respectively. The interesting result is that these angles experiment further increases in the doped coatings, reaching  $115^\circ$  for CrN+Cu and  $117^\circ$  for the TiN+Cu. In general, copper leads to higher increases, while silver provides intermediate values between the undoped and the Cu-doped cases.

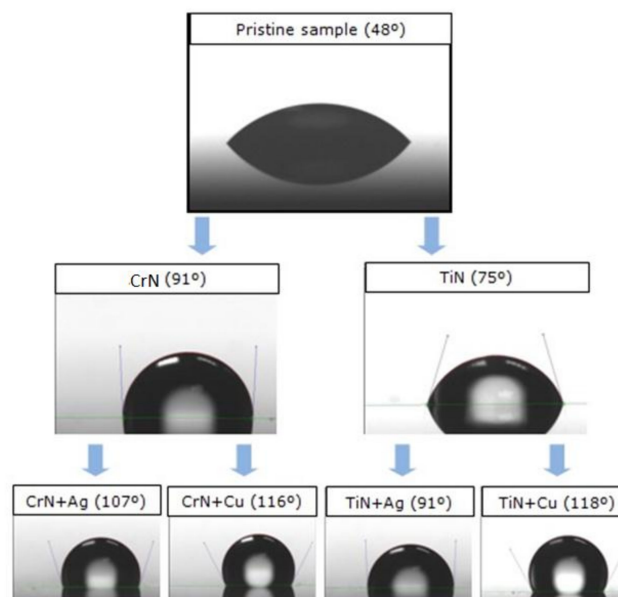


**Figure 9.** Wettability tests: contact angle images of the different undoped and doped coatings.

The changes in the surface roughness, and the presence of metal droplets, are responsible for the changes in the surface energy and the wettability. Accordingly, the lower surface energy for copper leads to higher contact angle values [26].

### 3.5. Antibacterial Efficacy Results

Finally, Table 3 collects the results obtained in the test for antimicrobial activity and efficacy. The values of the R factor were in all cases—except in the case of TiN+Ag against *S. aureus*—much higher than two, which was the threshold value established in the JIS Z 2801:2010 Standard to consider a surface as bactericide.

In the case of the antibacterial test of TiN+Ag against *S. aureus*, the growth of the bacteria on the TiN samples that were used as a reference was lower than expected, reducing the value of the R factor even though the coating produced the total elimination of the bacteria after 24 h. This bacteriostatic or antibacterial effect has been observed previously for titanium nitride, which is attributed to the formation of small amounts of titanium oxide during the deposition process of the samples used as the reference in the tests [27,28].

**Table 3.** Results of the JIS Z 2801:2010 Standard for CrN and TiN-based coatings.

Sample	R factor	
	<i>E. coli</i>	<i>S. aureus</i>
CrN+Ag	4.3	4.7
CrN+Cu	5.7	4.7
TiN+Ag	5.7	2.1
TiN+Cu	5.7	4.1

In all of the cases, the number of bacteria in the treated samples was 0 after the tests, highlighting the high antibacterial effects of the silver and copper deposited by PVD. The different values of  $R$  were related to the growth of the bacteria in the reference samples, given that  $R = \log(B/C)$ , where  $B$  = the number of colony-forming units in the reference samples (TiN or CrN) after 24 h and  $C$  = the number of colony-forming units in the treated samples (TiN+Ag/Cu, CrN+Ag/Cu) after 24 h.

#### 4. Conclusions

Silver and copper-doped CrN and TiN coatings were deposited over common glazed ceramic tiles using cathodic arc PVD (CA-PVD).

As expected, the GD-OES profiles showed that the doped layer was about 100 nm on the surface of the coatings, and the concentration of these metals (Ag or Cu) was about a 20%. Particles between tens of nanometers and few micrometers in the size of these metals were heterogeneously distributed all over the surface. The ceramic matrix (TiN or CrN) was not able to dissolve all of the metal; thus, the antibacterial metal segregates in the grain boundary, producing a composite structure [13,14]. The presence of microdroplets produced during the evaporation also leads to the formation of this kind of layer structure.

The coatings have a relatively higher hardness in comparison to common glazing, which is not lowered by the soft metal dopants. The roughness of the samples increased due to the treatments. This increment is almost negligible, and is due to the deposition of microdroplets on the surface during the PVD process. The deposited coatings showed a good adhesion, remaining adhered to the surface until the substrate fracture, although the silver doped coatings had lower values of critical loads, particularly in the case of the TiN-based coatings. An anomalous behavior has been observed on the TiN+Ag samples, which presented low adhesion values. This behavior was attributed to problems during the cleaning process.

The contact angle between deionized water and the different surfaces was much higher on the treated samples than on the uncoated ones. The Ag or Cu-doped CrN samples had higher contact angles than the common CrN and TiN, reaching 115° for the CrN+Cu and 117° in the case of the TiN+Cu, respectively. The low energy of the antibacterial metals and the roughness produced by the microdroplets were responsible for these changes.

The antibacterial effect for the coatings was very high. Following the JIS Z 2801:2010 Standard [24], all of the treatments, except TiN+Ag against *S. aureus*, showed a value of the  $R$  factor higher than four, where two is the threshold value. The presence of metal particles in the surface produces the liberation of metallic ions that prevent the bacteria proliferation.

As a general conclusion, the doped PVD coatings keep the high mechanical properties of the undoped ones, and show a high antibacterial effect, according to the JIS Z 2801:2010 standard. The use of these coatings in the clinical environment could reduce the proliferation of bacteria in the treated surfaces.

**Author Contributions:** Conceptualization, Rafael Rodríguez, Jose Antonio García; Methodology, Gonzalo García Fuentes, Rafael Rodríguez; Validation, Refael Rodríguez, Fonzalo García Fuentes; Formal Analysis, Javier Osés, Joseba Esparza, José Fernández Palacio; Investigation, Javier Osés, Joseba Esparza, José Fernández Palacio; Resources, Joseba Esparza, José Fernández Palacio; Data Curation, Writing-Original Draft Preparation, Javier Osés; Writing-Review & Editing, Javier Osés, José Fernández Palacio, Rafael Rodríguez; Supervision, Jose Antonio

García, Rafael Rodríguez; Project Administration, Rafael Rodríguez; Funding Acquisition, José Antonio García, Gonzalo García Fuentes.

**Funding:** This research was funded by Departamento de Innovación, Empresa y Empleo from Gobierno de Navarra and Fondo Europeo de Desarrollo Regional. Project EUROINNOVA EP-2 NANOCONS (IIM10784.R11-02182).

**Conflicts of Interest:** The authors declare no conflict of interest.

## References

1. Boyce, J.M. Environmental contamination makes an important contribution to hospital infection. *J. Hosp. Infect.* **2007**, *65*, 50–54. [[CrossRef](#)]
2. Rodrigues da Costa, A.; Kothari, A.; Bannister, G.C.; Blom, A.W. Investigating Bacterial Growth in Surgical Theatres: Establishing the Effect of Laminar Airflow on Bacterial Growth on Plastic, Metal and Wood Surfaces. *Ann. R. Coll. Surg. Engl.* **2008**, *90*, 417–419. [[CrossRef](#)] [[PubMed](#)]
3. Weber, D.J.; Rutala, W.A.; Miller, M.B.; Huslage, K.; Sickbert-Bennett, E. Role of hospital surfaces in the transmission of emerging health care-associated pathogens: Norovirus, Clostridium difficile, and Acinetobacter spp. *Am. J. Infect. Control* **2010**, *38*, S25–S33. [[CrossRef](#)] [[PubMed](#)]
4. Weber, D.J.; Rutala, W.A. Self-disinfecting surfaces: Review of current methodologies and future prospects. *Am. J. Infect. Control* **2013**, *41*, S31–S35. [[CrossRef](#)] [[PubMed](#)]
5. Borkov, G. *Use of Biocidal Surfaces for Reduction of Healthcare Acquired Infections*; Springer: Cham, Switzerland, 2014; ISBN 978-3-319-08056-7.
6. Alexander, J.W. History of the medical use of silver. *Surg. Infect.* **2009**, *10*, 289–292. [[CrossRef](#)] [[PubMed](#)]
7. Grass, G.; Rensing, C.; Solioz, M. Metallic copper as an antimicrobial surface. *Appl. Environ. Microbiol.* **2011**, *77*, 1541–1547. [[CrossRef](#)] [[PubMed](#)]
8. Kumar, R.; Münstedt, H. Silver ion release from antimicrobial polyamide/silver composites. *Biomaterials* **2005**, *26*, 2081–2088. [[CrossRef](#)] [[PubMed](#)]
9. Panacek, A.; Kvítek, L.; Pucek, R.; Kolar, M.; Vecerova, R.; Pizúrova, N.; Sharma, V.K.; Nevecna, T.; Zboril, R. Silver colloid nanoparticles: Synthesis, characterization, and their antibacterial activity. *J. Phys. Chem. B* **2006**, *110*, 16248–16253. [[CrossRef](#)] [[PubMed](#)]
10. Moreno, A.; Lázaro, V.; Mateu, A.; Reig, Y. Innovations and New Trends in Ceramic Tile Decoration. *Adv. Sci. Technol.* **2010**, *68*, 165–175. [[CrossRef](#)]
11. Wan, Y.Z.; Raman, S.; He, F.; Huang, Y. Surface modification of medical metals by ion implantation of silver and copper. *Vacuum* **2007**, *81*, 1114–1118. [[CrossRef](#)]
12. Osés, J.; Palacio, J.F.; Kulkarni, S.; Medrano, A.; Garcia, J.A.; Rodriguez, R. Antibacterial PVD coatings doped with silver by ion implantation. *Appl. Surf. Sci.* **2014**, *310*, 56–61. [[CrossRef](#)]
13. Kelly, P.J.; Li, H.; Benson, P.S.; Whitehead, K.A.; Verran, J.; Arnell, R.D.; Iordanova, I. Comparison of the tribological and antimicrobial properties of CrN/Ag, ZrN/Ag, TiN/Ag, and TiN/Cu nanocomposite coatings. *Surf. Coat. Technol.* **2010**, *205*, 1606–1610. [[CrossRef](#)]
14. Audronis, M.; Jimenez, O.; Leyland, A.; Matthews, A. The morphology and structure of PVD ZrN–Cu thin films. *J. Phys. D Appl. Phys.* **2009**, *42*, 085308. [[CrossRef](#)]
15. Yao, S.H.; Su, Y.L.; Kao, W.H.; Cheng, K.W. Evaluation on wear behavior of Cr–Ag–N and Cr–W–N PVD nanocomposite coatings using two different types of tribometer. *Surf. Coat. Technol.* **2006**, *201*, 2521–2526. [[CrossRef](#)]
16. Incerti, L.; Rota, A.; Valeri, S.; Miguel, A.; García, J.A.; Rodríguez, R.J.; Osés, J. Nanostructured Self Lubricating CrN–Ag films deposited by Arc Discharge and PVD Magnetron Sputtering. *Vacuum* **2011**, *85*, 1108–1113. [[CrossRef](#)]
17. Wang, J.; Gong, X.; Hai, J.; Li, T. Synthesis of silver–hydroxyapatite composite with improved antibacterial properties. *Vacuum* **2018**, *152*, 132–137. [[CrossRef](#)]
18. Sikora, P.; Cendrowski, K.; Markowska-Szczupak, A.; Horszczaruk, E.; Mijowska, E. The effects of silica/titania nanocomposite on the mechanical and bactericidal properties of cement mortars. *Constr. Build. Mater.* **2017**, *150*, 738–746. [[CrossRef](#)]
19. Berg, G.; Friedrich, C.; Broszeit, E.; Berger, C. Development of chromium nitride coatings substituting titanium nitride. *Surf. Coat. Technol.* **1996**, *86*, 184–191. [[CrossRef](#)]

20. Cai, F.; Huang, X.; Yang, Q. Mechanical properties, sliding wear and solid particle erosion behaviors of plasma enhanced magnetron sputtering CrSiCN coating systems. *Wear* **2015**, *324*, 27–35. [[CrossRef](#)]
21. Doerner, M.F.; Nix, W.D. A method for interpreting the data from depth-sensing indentation instruments. *J. Mater. Res.* **1986**, *1*, 601–609. [[CrossRef](#)]
22. Doerner, M.F.; Nix, W.D. Stresses and deformation processes in thin films on substrates. *Crit. Rev. Solid State Mater. Sci.* **1988**, *14*, 225–268. [[CrossRef](#)]
23. Zhou, B.; Prorok, B. An Improvement of the Doerner-Nix Function for Substrate Effects in Ultrathin Films. *MRS Proc.* **2008**, *1086*. [[CrossRef](#)]
24. *JIS Z 2801:2010 Antibacterial Products—Test for Antibacterial Activity and Efficacy*; Japanese Standards Association: Mita, Japan, 2010.
25. Yate, L.; Martínez-de-Olcoz, L.; Esteve, J.; Lousa, A. Control of the bias voltage in d.c. PVD processes on insulator substrates. *Vacuum* **2009**, *83*, 1287–1290. [[CrossRef](#)]
26. Blanco, D.; Viesca, J.L.; Mallada, M.T.; Ramajo, B.; González, R.; Hernández Battez, A. Wettability and corrosion of [NTf<sub>2</sub>] anion-based ionic liquids on steel and PVD (TiN, CrN, ZrN) coatings. *Surf. Coat. Technol.* **2016**, *302*, 13–21. [[CrossRef](#)]
27. Groessner-Schreiber, B.; Hannig, M.; Dück, A.; Griepentrog, M.; Wenderoth, D.F. Do different implant surfaces exposed in the oral cavity of humans show different biofilm compositions and activities? *Eur. J. Oral Sci.* **2004**, *112*, 516–522. [[CrossRef](#)] [[PubMed](#)]
28. Kelly, P.J.; Li, H.; Benson, P.S.; Whitehead, K.A.; Verran, J.; Arnell, R.D.; Iordanova, I. A study of the antimicrobial and tribological properties of TiN/Ag nanocomposite coatings. *Surf. Coat. Technol.* **2009**, *204*, 1137–1140. [[CrossRef](#)]



© 2018 by the authors. Licensee MDPI, Basel, Switzerland. This article is an open access article distributed under the terms and conditions of the Creative Commons Attribution (CC BY) license (<http://creativecommons.org/licenses/by/4.0/>).